JAAS

ROYAL SOCIETY OF CHEMISTRY

TECHNICAL NOTE

View Article Online
View Journal | View Issue

Cite this: *J. Anal. At. Spectrom.*, 2023, **38**, 57

Light-element sensitive in-air millibeam PIXE setup for fast measurement of atmospheric aerosol samples†

Shafa Aljboor, [ab] Anikó Angyal, [b] Dávid Baranyai, [c] Enikő Papp, [b] Máté Szarka, [b] Zita Szikszai, [b] István Rajta, [d] István Vajda [d] and Zsófia Kertész *[b]

A sensitive in-air millibeam PIXE setup has recently been installed at the external beamline of the ATOMKI 2 MV Tandetron accelerator (Debrecen, Hungary) for high-throughput analysis of samples with short measurement time (100–300 s). The setup contains an X-ray detector cluster, 2 positioning lasers, a digital camera-microscope, an *x*–*y* precision stage, a Faraday cup and a measurement control and data acquisition system. By default, the detector cluster incorporates three 65 mm^2 SDD detectors with 12.5 micrometer Be window and one 30 mm^2 SDD with an ultra-thin Si_3N_4 window. In a 2 l min^{-1} He flow, the system enables the simultaneous detection of X-rays from 0.35 keV to 26 keV, *i.e.* elements with $Z > 6$. The analytical characteristics are demonstrated further through analysis of reference materials. The effect of He saturation level on the calculated concentration of light elements is also shown. The new in-air PIXE system is suitable for the quantitative elemental characterization of both thin and thick samples with high sensitivity and good efficiency. The broad elemental range makes it particularly suitable for the analysis of atmospheric aerosol samples and archaeological, museum objects.

Received 29th August 2022
Accepted 26th October 2022

DOI: 10.1039/d2ja00291d

rsc.li/jaas

1. Introduction

Accelerator-based fundamental and applied research have always been an area of utmost importance in ATOMKI, Debrecen since its founding in 1954. The ATOMKI Accelerator Centre (AAC)[1] which hosts several small-scale particle accelerators is one of the top research infrastructures of Hungary.[2] One of the main research areas is ion beam analysis and its applications in the fields of environmental research, biomedicine, geology, materials & surface science (including ion beam induced damage investigations and proton beam lithography), radiation chemistry and heritage science.[3–7] In 2019, after 48 years of reliable operation the 5 MV Van de Graaff accelerator (VdG5) was shut down due to the deteriorating conditions of both the accelerator and its accommodating building. In the meantime, as part of an infrastructure development program, a new 2 MV Tandetron accelerator by High Voltage Engineering Europa B.V was installed in 2014,[8] and thus development and construction of new beamlines have been started. One of the first four beamlines operational at the Tandetron was the external millibeam which was used for the irradiation of different polymers and liquids at that time.[9,10]

Particle Induced X-ray Emission (PIXE), complemented by other (ion beam) analytical techniques is still widely used in several multidisciplinary research fields despite the advances of competitive methods like ICP-MS, XRF or synchrotron-based techniques.[11,12,13] At present, the two main application areas of PIXE in ATOMKI is the characterization of urban atmospheric aerosol pollution and archaeometry. The main advantages of PIXE are: it is fast, fully quantitative without using standards, covers a wide range of elements ($Z = 6$–92), usually does not require any sample preparation, very small sample mass in enough for the analysis, and non-destructive if carefully applied.[14,15] Earlier, aerosol samples were measured in-vacuum in the bulk-PIXE chamber of the VdG5, while museum and archaeological specimens were studied at the scanning nuclear microprobe either in-vacuum or in-air, depending on the object and the required analytics. In both cases, in-air systems have many advantages: easy sample handling, quick specimen exchange and positioning, reduced charging effects and heat induced damage, no evaporation of volatile elements, and the possibility to measure vacuum sensitive or large objects not fitting into a vacuum chamber. The 'Achilles heel' of in-air setups is the measurement of the beam dose. The tight geometry and the atmospheric environment do not allow the use of best practices which work well in vacuum. At the ion beam

[a]*University of Debrecen, PhD School in Physics, Debrecen, Hungary*
[b]*Laboratory for Heritage Science, Institute for Nuclear Research, Debrecen, Hungary. E-mail: kertesz.zsofia@atomki.hu*
[c]*University of Debrecen, Faculty of Informatics, Debrecen, Hungary*
[d]*Tandetron Laboratory, Institute for Nuclear Research, Debrecen, Hungary*

† Electronic supplementary information (ESI) available. See DOI: https://doi.org/10.1039/d2ja00291d

facilities around the world, several different methods have been implemented for monitoring the beam dose including simultaneous RBS measurements[16,17] monitoring the exit window[18] or applying electrostatic deflection systems,[19] beam profile monitors[20] and beam choppers.[21]

Because of these reasons we seized the opportunity to create an external millibeam PIXE setup which fulfils the requirements of advanced atmospheric aerosol and heritage science research. The new in-air PIXE setup together with the new ion beam analytical vacuum chamber, the re-built scanning nuclear microprobe and a recently installed scanning nuclear nanoprobe makes the ion-beam analytical arsenal of the ATOMKI Tandetron Laboratory complete.

Although researchers working in the field of ion beam analysis (IBA) like to refer IBA methods as non-destructive, it is only true within certain limits.[22–24] Recently, a number of studies were published which deal with the so called 'safe boundaries' of ionizing radiation on different materials.[25,26] Their findings are that above a certain irradiation fluence irreversible changes might occur. The probability and the magnitude of beam induced alteration/damage is depending on the type of ion, the energy and the fluence of the beam, the dose and the material. Therefore, in order to remain on the safe side, one should work with relatively small beam fluences (*e.g.*, 0.5–1 μC cm^{-2}) without losing analytical information. One way to achieve this goal is to increase significantly the efficiency of detection.

With the advancement of Silicon Drift X-ray detectors (SDD), with the favorable properties for X-ray spectrometry, such as compact size, high count rates and relatively low price, it became possible to develop multi-detector arrays with huge solid angles. In the past years this have been the direction of development at external beam facilities in the field of detection.[21,27–29]

Another aspect which had to be taken into consideration was the limited availability of beamtime. Besides ion beam applications, numerous projects in nuclear physics, nuclear astrophysics, planetary science and materials sciences are running at the various beamlines exploiting the new possibilities provided by the state-of-the-art infrastructure of the ATOMKI Tandetron Laboratory.[30–32]

In this paper we give a detailed description of the newly developed external-PIXE setup and present results obtained by PIXE measurements on various reference materials.

2. The ATOMKI in-air millibeam PIXE set-up

The in-air PIXE setup was built on the left 45° 'external' beamline of the Tandetron.[1] Since this is the only in-air beamline, it is shared among all of the users, who has many different measurement setups and systems. Therefore, we had to develop a compact, mobile setup which can be easily fitted to and removed from the beamline end.

The setup is built on a table with 100 cm × 100 cm dimensions. It contains a multi-detector cluster with sample positioning system by RaySpec Ltd, a precision *x*–*y* stage, and a Faraday cup. The setup is connected to the beamline end with KF-40 bellows.

The extraction window is a 200 nm thick silicon nitride membrane by Norcada Inc. with 2 mm × 2 mm window size. In our experience and that of others, silicon nitride films are reliable and durable window materials.[20,28,33] At the external microbeam the same extraction window is used and the foil had to be replaced only once due to thinning since 2014. Before the exit window, the beam passes through a series of collimators. Samples are positioned at 10 mm distance from the exit window. By default, the detector cluster incorporates three 65 mm^2 Silicon Drift Detectors (SDD) with 12.5 micrometer thick Be window and one 30 mm^2 SDD with an ultra-thin Si_3N_4 window. The SDD detectors has a thickness of 450 μm with 129 eV (FWHM) energy resolution for the 5.9 keV line of Mn. The ultra-thin windowed (UTW) detector is equipped with a pair of 4 cm long permanent magnets of 1 T magnetic field which prevents the scattered protons from entering the detector. Absorber foils are used in front of the Be-windowed detectors in order to attenuate the low-energy X-ray lines and to protect the detectors, as well. All detectors are positioned at 135° geometry. The distance of the UTW detector from the sample is 80 mm while the Be-windowed detectors are positioned at 12 mm from the target. The 3 Be-windowed detectors together cover ~0.45 sr solid angle. He flow can be introduced in front of the UTW SDD, if needed. In a 2 l min^{-1} He flow, the system enables the detection of X-rays down to 0.35 keV, *i.e.* elements down to N. A multi-channel digital X-ray signal processor 'xMAP' by XIA LLC is used for data acquisition.

The experimental arrangement allows one ore more SDD to be replaced by a Si(Li) detector when the analysis requires it, since Si(Li) detectors are more sensitive in the high X-ray energy region. In addition, the detection system can be complemented with a compact HpGe detector with 50% efficiency and particle detectors, too. Fig. 1A shows the SDD detector cluster while on Fig. 1B and C detector arrangements with a HpGe gamma detector and a Si(Li) X-ray detector can be seen, respectively.

Samples are mounted perpendicular to the beam on an *x*–*y* precision stage. Usually, the samples are scanned in front of the beam (on a few cm^2 area) in order to reduce the risk of possible degradation and to increase the analyzed area. Sample change and the scanning can be preprogrammed and can be also controlled remotely in a semi-automatic way. Two lasers and a digital camera-microscope are dedicated for sample positioning. This latter subsystem is used to adjust the alignment of the setup (*i.e.* position of samples relative to detectors) every time when it is mounted on the beamline. On the other hand, samples are continuously monitored during the measurements *via* the camera-microscope.

In the case of aerosol samples, when the sample is thin enough for the beam to pass through, the irradiation dose is measured by integrating the current on a Faraday cup placed behind the filters.[28] The Faraday cup is coated with 2 layers of thick carbon foil ensuring that no X-rays are emitted from it.

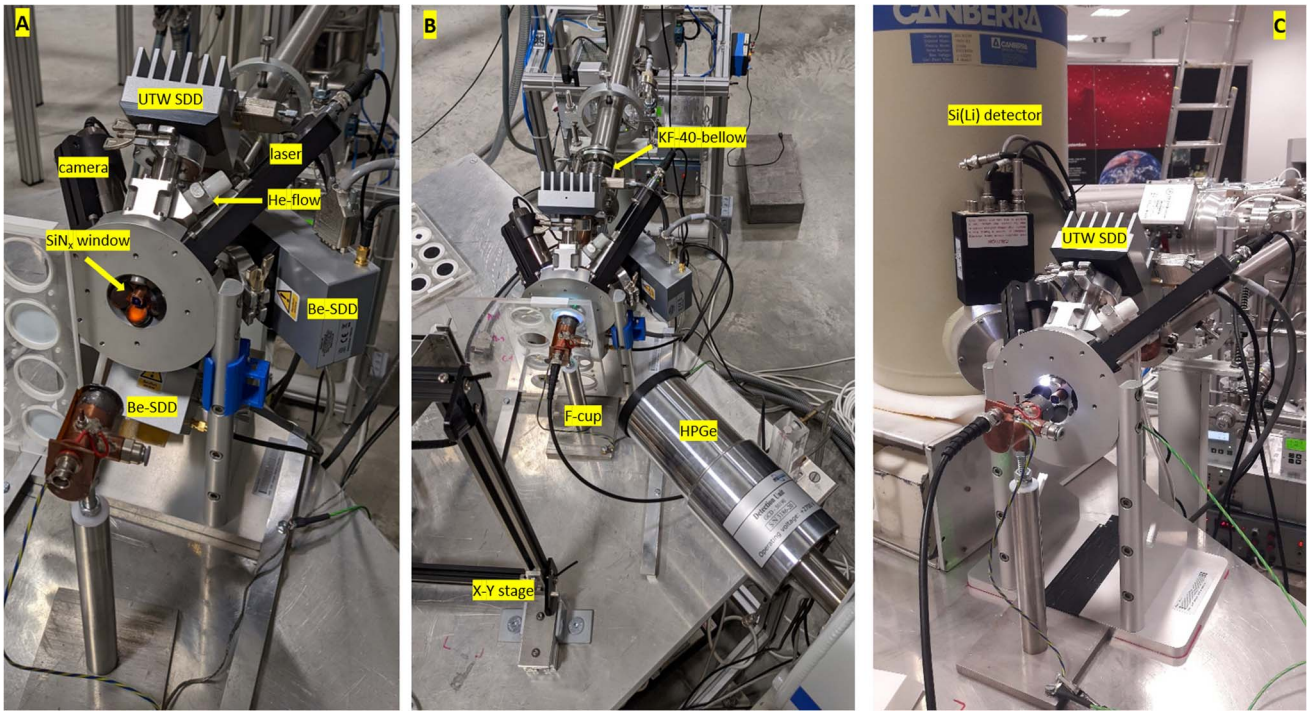

Fig. 1 Pictures of the new external millibeam PIXE set-up. (A) (left) default SDD cluster with UTW SDD and 3 Be-windowed SDDs equipped with Kapton absorbers. (B) (center) SDD cluster with a HpGe gamma detector by Baltic Scientific during the measurement of aerosol samples. (C) (right) detector arrangement with a Canberra Si(Li) and the UTW SDD.

3. Performance of the new in-air PIXE setup

3.1. Atmospheric aerosol samples

For in-air PIXE measurements the aerosol filter samples are irradiated with a proton beam of 2.5 MeV energy on target and of 10–70 nA current. Kapton absorber foils of 125 μm thickness are applied on the 3 Be-windowed SDDs. The obtained spectra are evaluated by the GUPIXWIN program code.[34] Aerosol samples collected on Teflon/PTFE, quartz fiber and nucleopore polycarbonate (PC) filters have been studied so far during 4 measurement campaigns. These are the commonly used filter types in atmospheric particulate matter pollution studies. The accumulated charge on all samples were 10 μC. In the case of quartz and PTFE filters, lower currents (15–25 nA) were applied. The quartz filters were analyzed under normal atmospheric conditions, since the high Si content of the filter material does not allow the accurate analysis of light elements. In the case of PTFE and polycarbonate filter samples, 2 l min^{-1} He flow in front of the UTW detector was applied. The samples were scanned in front of the beam in an area of 10 mm × 10 mm.

Table 1 summarizes the detection limits (LOD) calculated for the different filter types for the UTW SDD and the 3-SDD cluster (*i.e.* sum of the 3 identical detectors). LOD values were calculated by the GUPIXWIN program,[34] which is based on 3 times the standard deviation of the background area over a 1 FWHM region around the peak centroid. For more details see ESI.† LODs presented here were determined for blank filters in order to avoid the effect of intensive neighboring peaks, overlapping peaks, pile-ups, escape peaks, *etc.* Nevertheless, LODs obtained for the real aerosol samples were very similar. For comparison, LODs achieved with the previous, in-vacuum PIXE setup[35] are also shown. The typical measurement conditions in the vacuum chamber were the following: 2 MeV H^+ beam, 30–50 nA current, 40 μC accumulated charge for polycarbonate, 20 μC accumulated charge for PTFE and quartz filters, detector: 50 mm^2 Si(Li) with 12 μm Be window and 24 μm mylar absorbent. The beam current had to be reduced below 10 nA in the case of PTFE and quartz fiber filters because of the increased high-energy background caused by Compton scattering of gamma radiation of F within the detector (PTFE) and sample charging (quartz).

The table shows that we reached excellent detection limits with the new SDD detector cluster using 25–50% of the irradiation dose compared to the in-vacuum system. The difference between the old in-vacuum setup and the new in-air setup is most striking in the case of quartz and PTFE filters, when LODs were improved by several factors. In addition, the range of analyzed elements have been significantly extended in the direction of low-*Z*. Due to the relatively smaller thickness of SDDs compared to Si(Li) detectors, the Compton background is significantly reduced, improving LODs by factors of 5–15 for medium and high *Z* elements.[28] For quartz and polycarbonate filters the higher beam energy, the increased solid angle and the reduction of sample charging might lead to the better LODs of heavier elements.

The quality of the PIXE analysis is checked by measuring reference materials. PIXE spectra collected on NIST SRM2783

Table 1 Detection limits in ng cm^{-2} determined for different filter blanks using SDD detectors of the new setup. Measurement conditions: 2.5 MeV H$^+$ beam, 10 μC collected charge. The right column of the table contains LODs of the old in-vacuum PIXE setup as a comparison (conditions: 2 MeV H$^+$ beam, 20/40 μC accumulated charge, * 1.8 MeV H$^+$ beam)

		UTW SDD			3-SDD cluster			Si(Li)		
		Quartz	PTFE/Teflon	Polycarbonate	Quartz	PTFE/Teflon	Polycarbonate	Quartz	PTFE/Teflon*	Polycarbonate
Element	X-ray energy (keV)	Air	He	He	Air	He	He	In-vacuum		
N	0.39		67	68.3						
O	0.525		1332	124						
F	0.68		721	30.9						
Na	1.04		35	9.1						
Mg	1.25		18	8.1						
Al	1.49		14.3	7.4					12.7	15.6
Si	1.74	1393	12.5	7					5.8	6.7
P	2.01	100	23	13.2					4.4	4.9
S	2.31	47.5	16	7.9	20.2	14.0	9.0	98.0	3.0	3.3
Cl	2.62	40.0	15.5	8.7	10.7	8.0	8.0	25.5	2.5	2.7
K	3.31	23.4	17.2	9.8	6.3	6.4	5.7	7.7	1.6	1.8
Ca	3.69	14.9	16.8	6.4	1.5	1.1	1.0	9.9	1.2	1.4
Ti	4.51	11.5	9	7.7	1.2	1.1	0.9	4.6	1.7	1.0
V	4.95	10.2	13	8.1	0.9	0.6	0.4	6.6	1.6	0.9
Cr	5.41	9.2	7.3	2.7	0.7	0.4	0.4	3.5	0.9	0.7
Mn	5.9	9.1	7.3	3.2	0.8	0.8	1.1	3.4	1.0	0.7
Fe	6.4	7.6	12.1	7.2	0.7	0.4	0.5	3.2	1.1	0.5
Co	6.93	8.6	16.8	5.1	0.9	0.6	0.6	4.0	1.2	1.0
Ni	7.47	6.3	18.1	9.4	0.6	0.3	0.3	2.8	1.4	0.5
Cu	8.04	7.1	26.4	5.9	0.6	0.3	0.3	2.7	2.6	0.5
Zn	8.63	6.9	30.3	12.3	0.6	0.3	0.3	2.9	2.4	0.6
As	10.51	16.2			1.1	0.8	0.4	5.1	8.7	1.1
Se	11.21	13.0			1.0	1.0	0.3	2.6	8.4	2.3
Br	11.91	19.4			0.7	1.3	0.2	4.6	8.4	2.5
Rb	13.38	35.1			0.9	2.4	0.7	5.2	23.4	6.4
Sr	14.14	51.6			1.0	2.2	0.4	13.6	31.7	7.1
Zr	15.75	100.0			2.1	5.6	1.4	12.2	49.1	8.4
Ba	4.46	43.0			4.2	2.7	2.3	16.3	4.9	4.5
Pb	10.54	32.0			1.9	1.6	0.6	13.8	18.8	5.4

reference material (particulate matter on filter media) is shown in Fig. 2. The measured elemental concentrations are presented in Table 2. All concentrations measured by both detectors were within the uncertainty of the certified/reference values.

As it is shown on the spectum of the UTW SDD, X-ray lines with energies as low as 0.39 keV (N) can be detected. This means that an estimate of the light element content of samples (except carbon) can be given with one short PIXE measurement. In

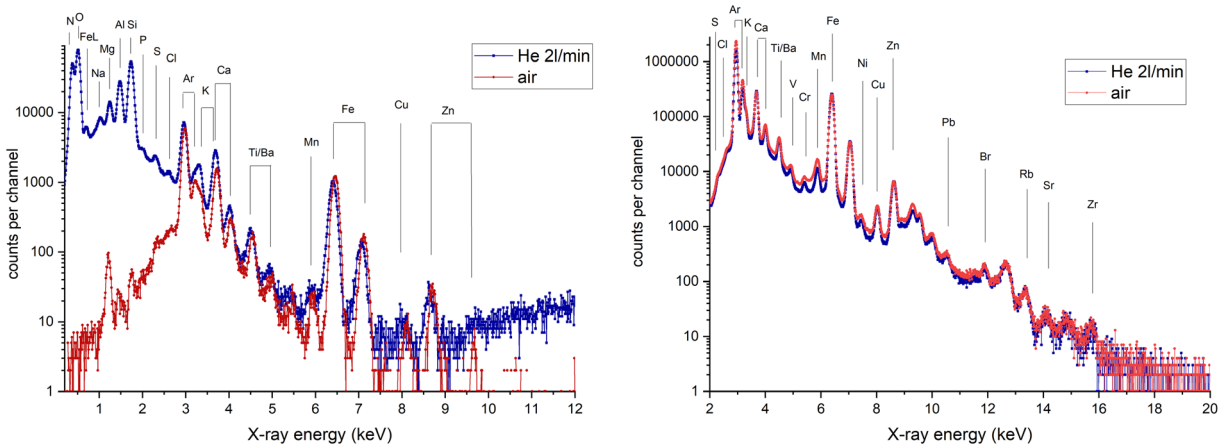

Fig. 2 PIXE spectra recorded on NIST SRM2783 by the UTW SDD (left) and the 3-SDD cluster (right) with and without He flow in front of the UTW detector. The main characteristic X-ray lines are indicated.

Table 2 Elemental concentrations of NIST SRM2783 reference material measured by the UTW-SDD and the 3-SDD cluster. Certified and reference (indicated with*) values are presented in the left columns of the table. Uncertainty originating from the spectrum fitting (fit error) and detection limits (LOD) are also included. In the case of Fe and Zn concentration values obtained for K and L lines are also given

	Certified/reference*		UTW SDD			3-SDD cluster		
	Conc. (ng cm^{-2})	SD (ng cm^{-2})	Conc. (ng cm^{-2})	Fit error (%)	LOD (ng cm^{-2})	Conc. (ng cm^{-2})	Fit error (%)	LOD (ng cm^{-2})
Na	186.7	10.0	180	18.3	19.1			
Mg	865.5	52.2	870	1.4	10.9			
Al	2330.3	53.2	2400	0.6	9.9			
Si*	5883.5	160.6	5990	0.5	8.6			
P			100	6.7	10.6			
S*	105.4	26.1	110	4.2	9.3	170	32.6	24.5
Cl			10	13.7	9.4			20.5
K	530.1	52.2	540	1.6	11.1	580	2.3	6.1
Ca	1325.3	170.7	1300	0.9	8.7	1360	0.8	1.7
Ti	149.6	24.1	135	3.8	5.6	136	1.7	1.0
V	4.9	0.6				7	17.2	1.4
Cr	13.6	2.5	10	31.7	5.4	10	6.9	0.5
Mn	32.1	1.2	40	12.0	4.6	27	2.8	1.4
Fe	2660.6	160.6	2510	1.1	8.3	2650	0.4	0.6
Fe L			2540	7.0	96.7			
Co	0.8	0.1			28.3			5.8
Ni	6.8	1.2			8.2	9	7.1	0.5
Cu	40.6	4.2	40	18.6	8.5	35	2.0	0.5
Zn	179.7	13.1	175	8.7	6.4	177	0.9	0.6
Zn L			195	20.5	33.5			
Rb*	2.4	0.6				2	45.4	1.6
Sr								1.2
Zr						10	26.2	1.4
Ba	33.6	5.0				40	10.5	16.7
Pb	31.8	5.4				35	12.4	2.6

addition, L lines of medium *Z* elements (*e.g.* Ti, Fe, Cu, Zn) can be evaluated which gives an extra information about the quality of the analysis. An example is given in Table 2, when the results for Fe K and L lines as well as Zn K and L show a very good match indicating that the parameters of the evaluation were correct.

3.2. PIXE characterization of glass samples

Although the operation of the system is optimized for the measurement of thin aerosol samples, it is possible to study thick specimen such as glass or metal samples with good sensitivity and efficiency. Since the current monitoring has not yet been solved for thick targets, the composition of the material is calculated by normalizing the measured concentrations to 100%. In order to be able to do so one must measure all main elemental components. As an example, results obtained for NIST SRM 610 reference glass and Corning A archeological reference glass[36] are presented (Tables S and S2 in ESI†). PIXE spectra recorded by the UTW SDD are shown in Fig. 3a and b.

Spectra collected by the UTW detector were evaluated 3 different ways using GUPIXWIN: fix matrix solution, iterated matrix solution using the common oxide formulae and iterated matrix solution for all elements independently (Table S3†). Measurement conditions were similar to that of the aerosol samples: 2.5 MeV H^+ beam, ~10 nA beam current, 2 l min^{-1} He flow, 2 μC accumulated charge. Spectra measured by the 3-SDD cluster were evaluated in the fixed matrix solution mode. All spectrum fitting methods resulted the same concentrations within uncertainty.

Naturally, for glasses and most minerals the oxygen content of a sample can be estimated from the common oxide formulae, and therefore it is not strictly necessary to measure oxygen. However, measuring directly the light element content gives an extra information about the operation of our system, and it can be used as a quality control of the measurement. On the other hand, there are samples with unknown N, O and F content when the capability of measuring low energy X-rays of 0.35–1 keV energies comes useful.

3.3 The influence of He-saturation level

During the measurements we apply He flow in order to detect light elements, and a flow rate of 2 l min^{-1} was proved to be optimal. The optimal He flux was determined by making a series of measurement on a thick (50 μm) Ni foil. The area under the Ar peak and the ratio of Ni K_α (7.474 keV) and Ni L_α (0.849 keV) lines were observed when increasing the He flux from 0 l min^{-1} to 4 l min^{-1} with 0.5 l min^{-1} steps. At 2 l min^{-1} flow rate the Ar peak disappeared and the Ni K_α/L_α peak ratio reached the plateau. Higher flow rates resulted in distortion of the PIXE spectra. The peaks widened and the background increased especially in the high energy region. Normally, the saturation of the volume before the detector with He should be

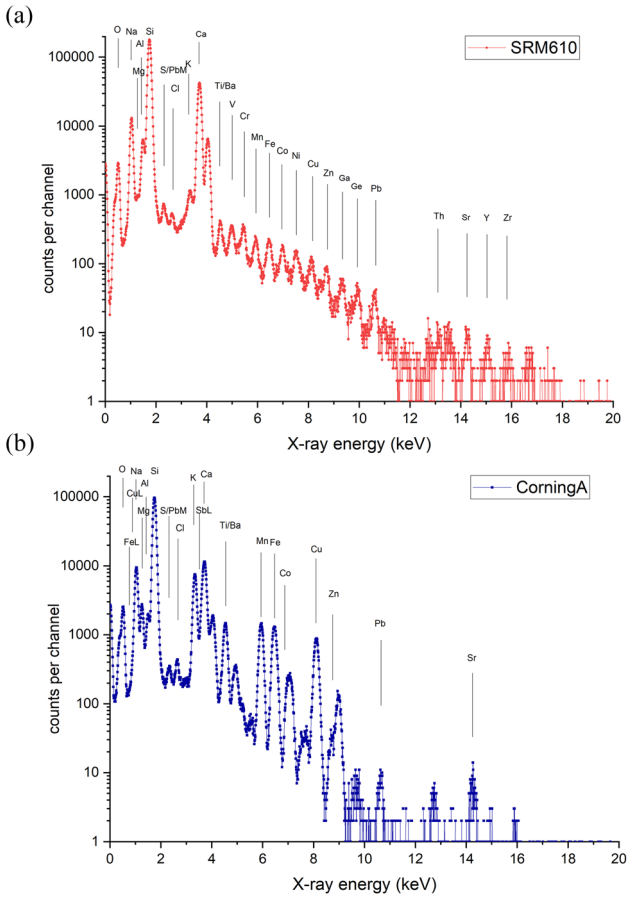

Fig. 3 (a) PIXE spectra recorded on NIST SRM610 reference glasses by the UTW SDD. The main characteristic X-ray lines are indicated. (b) PIXE spectra recorded on CorningA archeological reference glass by the UTW SDD. The main characteristic X-ray lines are indicated.

100%. However, in the spectra (Fig. 2 and 3) we see the presence of N. Although it is hardly visible, a very small amount of Ar was detectable in the spectra of the glasses, too. This can only originate from air which means that the level of saturation was not 100%. Indeed, the actual saturation level was 98.2%. Fig. 4 shows the variation of the calculated concentration as a function of X-ray energy when the saturation level is set to 99.9% in the evaluation software instead of the actual level of 98.2%. It was calculated for both thin (aerosol) and thick (glass) samples by GUPIXWIN. The overestimation of the saturation level causes the underestimation of the concentration values of lighter elements. The effect is very profound for O, for which the correct concentration is 11 times the erroneous one, still substantial for Na (2×), and there is only 16% difference for Si. Thus, the effect decreases steeply with the increase of X-ray energy and disappears for K upwards when the neglect of 1.7% air no longer results erroneous concentrations.

Changes in the calculated concentration values of light elements as well as FeL and ZnL lines in an aerosol sample while increasing the He saturation level from 96% to 99.9% in the evaluation software is presented in Fig. 5. The concentration was set to 1 for each element at the 96% level.

The modelled concentrations are decreasing exponentially with increasing saturation levels. The extent of change depends on the energy of X-ray lines, as it was demonstrated in Fig. 4. For very low-energy X-ray lines the decrease is significant, it can reach 98–99%. This is the case for O K (0.525 keV), Fe L (0.705 keV) or F K (0.677 keV) lines, while for the 2.62 keV K_α line of Cl the effect is negligible. Apparently, it is of primary importance to have a good estimate on the actual level of saturation because the presence of air even in a very low amount can alter the determined concentrations of light elements by several factors.

One solution to obtain the right concentrations of light elements such as Na, Mg and Al is to carry out measurements with other IBA techniques like backscattering spectrometry (BS) and particle induced gamma-ray emission (PIGE). PIGE is especially sensitive for these elements, and it is applied in many laboratories.[37,28] However, since PIGE cross sections are significantly (by orders of magnitude) lower than the cross sections of

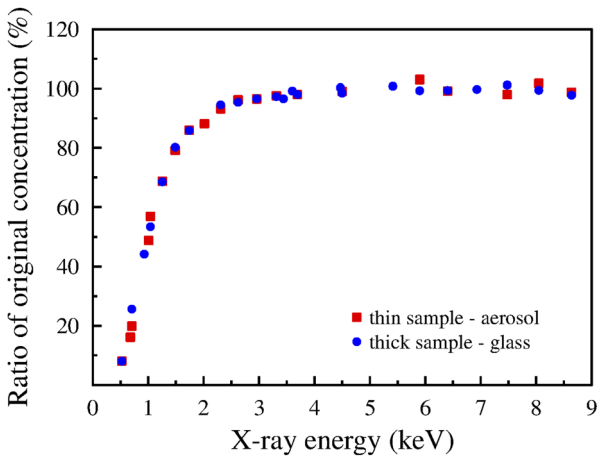

Fig. 4 Differences in the obtained concentration values for an aerosol (thin) and in a glass (thick) sample when the saturation of He is given as 99.9% instead of 98.2% (*i.e.*, saturation level for the 'original concentration') in the GUPIXWIN software.

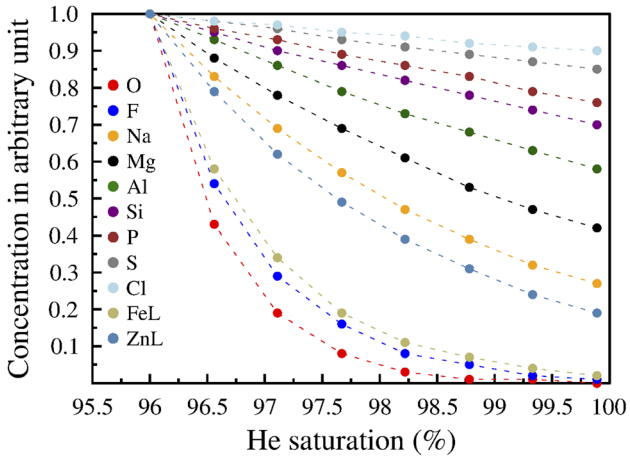

Fig. 5 Change in concentrations of light elements and low-energy L lines when the saturation level given in the evaluation software increased from 96% to 99.9%. The concentrations of each element were set to 1 at the 96% level.

PIXE, and the sensitivity of PIGE is more dependent on the beam energy, higher beam energies and much longer measurement times or higher beam doses are often needed. This is especially true in the case of aerosol samples when the concentrations are low and the quantities to be analyzed are very small. Applying PIGE parallel to PIXE would mean significant increase of the measurement time and increase of beam energy at least to 3 MeV (preferably higher). Due to several reasons including the protection of the UTW SDD detector and keeping the radiation level low in the accelerator hall, we prefer the beam energy at 2.5 MeV. Fortunately, in our case the PIXE spectrum itself offers the solution. In the case of aerosol samples, the filter material itself has a very strong signal in the spectrum of the UTW detector (see Fig. S1 in ESI†). PTFE filters contain fluorine in known concentrations, while oxygen in the spectrum of the polycarbonate filter samples originate predominantly from the filter material. The contribution of the particle deposit and the 1–2% air is negligible compared to the O content of the PC filters. Since the concentration of these elements is known or easily calculated, it serves as a kind of 'internal standard' for the estimation of the level of saturation. The only unknown parameter of the spectrum evaluation is the mixing ratio of He and air. It has to be set in such a way that the known concentrations of the characteristic elements of the filters are returned. Additionally, low-energy L-lines (typically, Fe, Cu, Zn) as well as the independent results of the 3-SDD cluster (or the actual other detectors(s)) function as secondary controls to the goodness of this approach.

In the case of thick samples, other methods have to be applied. One possibility is the simultaneous PIGE measurement. It has an advantage that PIGE can detect Li, Be, B and F with very good sensitivity besides the above-mentioned light elements (Na, Mg, Al, Si), too. If PIGE is not available, it is still possible to calculate concentrations for both the K and L lines of medium heavy elemental components at the same time. Good candidates are Ti, Mn, Fe, Ni, Cu, Zn, because the energy of their L lines is in the sensitive region while their K lines are not affected by the level of saturation. For glasses and minerals, the oxygen content can be estimated from the common oxide forms of elements, and then the approach described for the PC filters applies.

During our measurements the saturation of He changed between 97 and 99.5%.

4. Summary and conclusions

We have developed a mobile, flexible external millibeam PIXE measurement system which is capable of the elemental characterization of different sample types in a wide elemental range (N–U) with very good sensitivity. Thanks to the huge solid angle of the detector array and the fast-counting electronics, it is possible to collect enough information on a sample in much shorter time using less collected charge per sample than in conventional PIXE systems. For example, typical measurement time is now reduced to 100–300 s. This means that within a few minutes time information about the quantitative elemental composition of a sample for all elements heavier than C is obtained down to the trace element level in a non-destructive way.

If the analytical task requires, other ion beam analytical methods can be applied simultaneously since the measurement system can be easily supplemented with other detectors such as particle detectors (for BS) or HPGe (for PIGE).

For charge measurement the simplest possible methods are used: Faraday cup behind the sample for thin specimens and measurement of the actual beam current before and after irradiation of thick targets in order to have an estimate of the accumulated charge. In the case of thick targets, the normalization of the measured concentration to 100% gives very satisfactory results as long the sample does not contain unknown quantity of C.

The unique feature of the ATOMKI in-air PIXE system is the detection of very low energy X-rays including K-lines of light elements such as N, O and F and low-energy L-lines (*e.g.*, Fe, Cu, Zn). The detection of low-energy X-rays provide useful information about (1) the light element content of samples (2) measurement parameters and (3) measurement quality.

We have shown that knowing the He saturation level between the UTW detector and the target is very important because a few tenths of a percent fluctuation in the saturation leads to significant change in the obtained concentrations for light elements down from $Z = 17$. The measurement of these low-energy X-ray lines provides this information.

To our best knowledge this is the only in-air PIXE system operating at present which measures characteristic X-ray energies down to 0.35 keV and provides quantitative information for all measured elements. Earlier, qualitative light element detection by PIXE at the AGLAE in-air facility was reported by Calligaro *et al.*,[38] who used H_2 gas to fill up the space between the detector and the target.

The system, at its present state, is suitable for the complex bulk analysis of samples, which fulfils the requirements of modern, state-of-the-art atmospheric aerosol and heritage science research. With this new high-throughput PIXE system it became possible to analyze 100–200 samples in a 10–12 hours long shift, minimizing the usage of expensive and limited available beamtime and reducing significantly the cost of a measurement. In the future we would like to extend the capabilities in the direction of mapping of larger objects with a mm or better resolution.

Author contributions

Shafa Aljboor: writing – original draft preparation, investigation. Anikó Angyal: investigation, visualization, writing – reviewing and editing. Dávid Baranyai: software. Zsófia Kertész: conceptualization, methodology, writing – original draft preparation, supervision, visualization, investigation. Enikő Papp: investigation, writing – reviewing and editing. Máté Szarka: methodology, software, investigation, writing – reviewing and editing. Zita Szikszai: writing – reviewing and editing, resources. István Rajta: funding, writing – reviewing and editing. István Vajda: methodology, writing – reviewing and editing.

Conflicts of interest

The authors declare that they have no known competing interests.

Acknowledgements

The research was supported by the grant GINOP-2.3.3-15-2016-00005.

References

1 S. Biri, I. K. Vajda, P. Hajdu, R. Rácz, A. Csík, Z. Kormány, *et al.* The Atomki Accelerator Centre, *Eur. Phys. J. Plus*, 2021, **136**(2), 247. Available from: **http://link.springer.com/10.1140/epjp/s13360-021-01219-z**.

2 *TOP Research Infrastructures in Hungary 2021: TOP Research Infrastructures in Hungary and their Embeddedness in the European Research Infrastructure Landscape*, [Internet], ed. I. Szabó, National Research, Development and Innovation Office, 2021, Available from: **https://nkfih.gov.hu/english/top-rife-hungary2021**.

3 R. Huszank, L. Csedreki and Z. Török, Direct Trace Element Analysis of Liquid Blood Samples by In-Air Ion Beam Analytical Techniques (PIXE–PIGE), *Anal. Chem.*, 2017, **89**(3), 1558–1564.

4 Z. Kertész, Z. Szoboszlai, A. Angyal, E. Dobos and I. Borbély-Kiss, Identification and characterization of fine and coarse particulate matter sources in a middle-European urban environment, *Nucl. Instrum. Methods Phys. Res., Sect. B*, 2010, **268**(11–12), 1924–1928.

5 A. Simon, H. Matiskainen, I. Uzonyi, L. Csedreki, Z. Szikszai, Z. Kertész, *et al.* PIXE analysis of Middle European 18th and 19th century glass seals, *X-Ray Spectrom.*, 2011, **40**(3), 224–228.

6 A. Simon, F. Pászti, I. Uzonyi, A. Manuaba, Á. Z. Kiss and I. Rajta, Observation of surface topography using an RBS microbeam, *Nucl. Instrum. Methods Phys. Res., Sect. B*, 1998, **136–138**, 344–349.

7 E. Nady, G. Nagy and R. Huszánk, Functionalization of microfluidic devices by microstructures created with proton beam lithography, *Vacuum*, 2021, **190**, 110295.

8 I. Rajta, I. Vajda, G. y. Gyürky, L. Csedreki, Á. Z. Kiss, S. Biri, *et al.* Accelerator characterization of the new ion beam facility at MTA Atomki in Debrecen, Hungary, *Nucl. Instrum. Methods Phys. Res., Sect. A*, 2018, **880**, 125–130.

9 M. Szarka, S. Szilasi, B. Donczo, D. Sarkozy, I. Rajta and A. Guttman, The effect of simulated space radiation on the ***N*** -glycosylation of human immunoglobulin G1, *Electrophoresis*, 2018, **39**(22), 2872–2876.

10 R. Huszánk, G. Nagy, I. Rajta and A. M. Czeglédi, In-air proton beam irradiation induced radiolysis of methyl orange in aqueous solution, *Radiat. Phys. Chem.*, 2021, **180**, 109322.

11 W. Maenhaut, Present role of PIXE in atmospheric aerosol research, *Nucl. Instrum. Methods Phys. Res., Sect. B*, 2015, **363**, 86–91.

12 C. Jeynes. Ion beam analysis for cultural heritage. in *Spectroscopy, Diffraction and Tomography in Art and Heritage Science*. Elsevier; 2021. pp. 335–364.

13 M. Fedi, How a small accelerator can be useful for interdisciplinary applications part II: cultural heritage studies, *Eur. Phys. J. Plus*, 2021, **136**(4), 411.

14 F. Lucarelli, How a small accelerator can be useful for interdisciplinary applications: the study of air pollution, *Eur. Phys. J. Plus*, 2020, **135**(7), 538.

15 L. Giuntini, A review of external microbeams for ion beam analyses, *Anal. Bioanal. Chem.*, 2011, **401**(3), 785–793.

16 M. Xu, Y. J. Chu, G. F. Wang, M. L. Qiu and L. Zheng, An upgraded external beam PIXE setup for multielemental analysis of atmospheric aerosol samples, *X-Ray Spectrom.*, 2018, **47**(1), 79–85.

17 G. W. Grime, M. H. Abraham and M. A. Marsh, The new external beam facility of the Oxford scanning proton microprobe, *Nucl. Instrum. Methods Phys. Res., Sect. B*, 2001, **181**(1–4), 66–70.

18 D. Sokaras, E. Bistekos, L. Georgiou, J. Salomon, M. Bogovac, E. Aloupi-Siotis, *et al.* The new external ion beam analysis setup at the Demokritos Tandem accelerator and first applications in cultural heritage, *Nucl. Instrum. Methods Phys. Res., Sect. B*, 2011, **269**(5), 519–527.

19 J. Pallon, N. de La Rosa, M. Elfman, P. Kristiansson, E. J. C. Nilsson and L. Ros, A new quantitative X-ray system for micro-PIXE analysis, *X-Ray Spectrom.*, 2017, **46**(5), 319–324.

20 V. Palonen, K. Mizohata, T. Nissinen and J. Räisänen, External beam IBA set-up with large-area thin Si3N4 window, *Nucl. Instrum. Methods Phys. Res., Sect. B*, 2016, **380**, 11–14.

21 K. Isaković, M. Petric, Z. Rupnik, Ž. Šmit, P. Pelicon, M. Kelemen, *et al.* Upgrade of the external beamline at the microanalytical center of the Jožef Stefan Institute, *Nucl. Instrum. Methods Phys. Res., Sect. B*, 2022, **510**, 69–75.

22 M. Chiari, A. Migliori and P. A. Mandò, Investigation of beam-induced damage to ancient ceramics in external-PIXE measurements, *Nucl. Instrum. Methods Phys. Res., Sect. B*, 2002, **188**(1–4), 151–155.

23 T. Calligaro, V. Gonzalez and L. Pichon, PIXE analysis of historical paintings: Is the gain worth the risk?, *Nucl. Instrum. Methods Phys. Res., Sect. B*, 2015, **363**, 135–143.

24 A. Zucchiatti and F. Agulló-Lopez, Potential consequences of ion beam analysis on objects from our cultural heritage: An appraisal, *Nucl. Instrum. Methods Phys. Res., Sect. B*, 2012, **278**, 106–114.

25 L. Bertrand, S. Schöeder, D. Anglos, M. B. H. Breese, K. Janssens, M. Moini, *et al.* Mitigation strategies for radiation damage in the analysis of ancient materials, *TrAC, Trends Anal. Chem.*, 2015, **66**, 128–145.

26 K. Müller, Z. Szikszai, Á. Csepregi, R. Huszánk, Z. Kertész and I. Reiche, Author Correction: Proton beam irradiation induces invisible modifications under the surface of painted parchment, *Sci. Rep.*, 2022, **12**(1), 2431.

27 T. F. Silva, C. L. Rodrigues, N. Added, M. A. Rizzutto, M. H. Tabacniks, A. Mangiarotti, *et al.* Elemental mapping

of large samples by external ion beam analysis with sub-millimeter resolution and its applications, *Nucl. Instrum. Methods Phys. Res., Sect. B*, 2018, **422**, 68–77.

28 F. Lucarelli, G. Calzolai, M. Chiari, M. Giannoni, D. Mochi, S. Nava, *et al.* The upgraded external-beam PIXE/PIGE set-up at LABEC for very fast measurements on aerosol samples, *Nucl. Instrum. Methods Phys. Res., Sect. B*, 2014, **318**, 55–59.

29 L. Pichon, B. Moignard, Q. Lemasson, C. Pacheco and P. Walter, Development of a multi-detector and a systematic imaging system on the AGLAE external beam, *Nucl. Instrum. Methods Phys. Res., Sect. B*, 2014, **318**, 27–31.

30 D. v. Mifsud, Z. Juhász, P. Herczku, S. T. S. Kovács, S. Ioppolo, Z. Kaňuchová, *et al.* Electron irradiation and thermal chemistry studies of interstellar and planetary ice analogues at the ICA astrochemistry facility, *Eur. Phys. J. D*, 2021, **75**(6), 182.

31 G. Gyürky, Z. Halász, G. G. Kiss, T. Szücs, R. Huszánk, Z. Török, *et al.* Measurement of the ^{91}Zr(p,γ)^{92m}Nb cross section motivated by type Ia supernova nucleosynthesis, *J. Phys. G: Nucl. Part. Phys.*, 2021, **48**(10), 105202.

32 A. J. Krasznahorkay, M. Csatlós, L. Csige, J. Gulyás, A. Krasznahorkay, B. M. Nyakó, *et al.* New anomaly observed in 4He supports the existence of the hypothetical X17 particle, *Phys. Rev. C*, 2021, **104**(4), 044003.

33 Z. Török, R. Huszánk, L. Csedreki, J. Dani, Z. Szoboszlai and Z. Kertész, Development of a new in-air micro-PIXE set-up with in-vacuum charge measurements in Atomki, *Nucl. Instrum. Methods Phys. Res., Sect. B*, 2015, **362**, 167–171.

34 J. L. Campbell, N. I. Boyd, N. Grassi, P. Bonnick and J. A. Maxwell, The Guelph PIXE software package IV, *Nucl. Instrum. Methods Phys. Res., Sect. B*, 2010, **268**(20), 3356–3363.

35 I. Borbély-Kiss, E. Koltay, S. László, S. Gy and L. Zolnai, Experimental and theoretical calibration of a PIXE setup for K and L X-rays, *Nucl. Instrum. Methods Phys. Res., Sect. B*, 1985, **12**(4), 496–504.

36 L. Adlington, The Corning Archaeological Reference Glasses: New Values for "Old" Compositions, *Pap. Inst. Archaeol.*, 2017, **27**(1), 1–8.

37 X. F. Li, G. F. Wang, J. H. Chu and L. D. Yu, Charge integration in external PIXE–PIGE for the analysis of aerosol samples, *Nucl. Instrum. Methods Phys. Res., Sect. B*, 2012, **289**, 1–4.

38 T. Calligaro, J. D. MacArthur and J. Salomon, An improved experimental setup for the simultaneous PIXE analysis of heavy and light elements with a 3 MeV proton external beam, *Nucl. Instrum. Methods Phys. Res., Sect. B*, 1996, **109–110**, 125–128.